Structural Engineering and Mechanics, *Vol. 50, No. 6 (2014) 817-834*
DOI: http://dx.doi.org/10.12989/sem.2014.50.6.817

Structural performance of ferrocement beams reinforced with composite materials

Yousry B.I. Shaheen[a], Boshra A. Eltaly[*] and Samer G. Abdul-Fataha[b]

Civil Engineering Department, Faculty of Engineering, Minoufia University, Gamal Abdul-Nasser Street, Minufiya, Egypt

(Received January 4, 2014, Revised March 27, 2014, Accepted April 23, 2014)

Abstract. An experimental program was designed in the current work to examine the structural behavior of ferrocement beams reinforced with composite materials under three point loadings up to failure. The experimental program comprised casting and testing of twelve ferrocement beams having the dimensions of 120 mm width, 200 mm depth and 1600 mm length. The twelve beams were different in the type of reinforcements; steel bars, traditional wire meshes (welded and expanded wire meshes) and composite materials (fiberglass wire meshes and polypropylene wire meshes). The flexural performances of the all tested beams in terms of strength, ductility, cracking behavior and energy absorption were investigated. Also all the tested beams were simulated using ANSYS program. The results of the experimental tests concluded that the beam with fiber glass meshes gives the lowest first crack load and ultimate load. The ferrocement beam reinforced with four layers of welded wire meshes has better structural behavior than those beams reinforced with other types of wire meshes. Also the beams reinforced with metal wire meshes give smaller cracks width in comparing with those reinforced with non-metal wire meshes. Also the Finite Element (FE) simulations gave good results comparing with the experimental results.

Keywords: ferrocement; fiberglass mesh; polyethylene mesh; finite element method; nonlinear analysis

1. Introduction

Ferrocement is a special type of reinforced concrete. It consists of cement mortar matrix reinforced with closely spaced, multiple layers of mesh or fine rods completely impregnated with cement mortar. Ferrocement reinforcement is a wide variety of metallic reinforcing mesh materials; woven wire mesh, welded wire mesh and expanded metal mesh. Ferrocement has been used in a wide range of applications, including aqueducts, boats, buildings, bus shelters, bridge decks, food and water storage containers, irrigation structures, retaining walls, sculptures, roofing and traffic-caution signboards (Aboul-Anen *et al*. 2009, Ali 1995, Al-Kubaisy and Jumaat 2000, Robles-Austriaco *et al.* 1981). Also it is ideally suited as an alternative strengthening component for the rehabilitation of RC structures (Elavenil and Chandrasekar 2007, Fahmy *et al.* 1997, Jumaat and Alam 2006, Kaish *et al.* 2012, Mourad and shang 2012, Xiong *et al.* 2011).

∗Corresponding author, Ph.D., E-mail: boushra_eltaly@yahoo.com
[a]Professor, E-mail: ybishaheen@yahoo.com
[b]MS.c. Student, E-mail: Eng_samer18@yahoo.com

http://www.techno-press.org/?journal=sem&subpage=8 ISSN: 1225-4568 (Print), 1598-6217 (Online)

Several researches studied the behavior of the ferrocement element under different types of loads. Naaman and Shah (1971) studied the behavior of ferrocement under axial tension forces and found that ferrocement has a considerably higher bond area or specific surface than conventional reinforcement. Rajagopalan and Parameswaran (1975) studied the cracking and ultimate strength characteristics of ferrocement beams. They noticed that the ferrocement beam has better crack control and the smaller crack width than reinforced concrete. Walker (1995) presented experimental program included testing of six beams in flexure. His results showed that the first cracking of the beams was noticed at mid-span and with increasing load, the cracks spread towards the supports. Various types of beam specimens with various mesh types (hexagonal and square) were tested under two-point loadings system up to failure by Nassif and Najm (2004). Also they carried out a Finite Element (FE) model using ABAQUS program. Their results showed that the FE model gives accurate results comparing with their experimental results.

Fiberglass has excellent corrosion resistance, high tensile strength, high degree of flexibility and good non-magnetization properties. It can be widely used in building internal and external wall insulation, waterproofing, anti-crack and so on (Daniel and Shah 1994, Al-sayed and Al-hozaimy 1999). Harris *et al.* (1998) tested beams reinforced with hybrid FRP reinforcing bars and found that the ductility index of these beams were close to that of the beams reinforced with steel. Li and Wang (2012), Zhang and Huang (2009) studied the flexural behavior of concrete beams reinforced with GFRP and steel bars. The beam reinforced with GFRP has the best flexural behavior. Sakthivel and Jagannathan (2012) have introduced a new non-corrosive mesh material in ferrocement, namely the PVC-coated steel welded mesh ('P' mesh) and conducted studies on flexural strength. Additionaly Sakthivel and Jagannathan (2012) conducated a low-velocity impact study on 250 mm square fibrous ferrocement slab elements of 25 mm thick reinforced with PVC-coated welded mesh (three to four layers) and barchip olefin fibers (0.5%- 2.5% of volume of specimens). The energy absorbed by the FRF slabs was found to be higher than that of plain ferrocement slabs (cast with PVC mesh only). Also the impact energy increases with increasing in the number of mesh layers, and also increases with increasing in percentage of barchip fibers from 0.5% to 2.5%. Shaheen *et al.* (2013) studied the behavior of ferrocement channel beams under four point loadings until failure. The beams reinforced with various types of meshes; welded, expanded and fiberglass meshes. Their results indicated that the beam reinforced with welded wire mesh achieved higher first crack load, serviceability load, ultimate load and energy absorption than beams reinforce with expanded and fiberglass mesh.

The main objective of the current work is to examine the flexural behavior of ferrocement beams reinforced with composite material; fiberglass wire meshes and polyethylene wire meshes and comparing their behavior with ferrocement beams reinforced with traditional wire meshes. Twelve beams with different in the types of reinforcement were tested up to failure. Also the current research aims to simulate the tested beams by finite element ANSYS program to investigate their flexural behavior up to failure.

2. Experimental work

The current experimental program comprised casting and testing under flexure twelve beams. The beams have 120×200 mm cross section and 1600 mm length and reinforced with various types of reinforcing materials. The details of the test specimens are given in Fig. 1 and Table 1.

2.1 Properties of the used materials

Natural siliceous sand was used as the fine aggregate throughout the current research. The sieve analysis was done on the sand used for the ferrocement mortar mix and its results are presented in Table 2. Ordinary Portland cement was used and its chemical and physical properties were analyzed according to E.S.S. (2011) for concrete works. Fresh drinking water and free from impurities was used for mixing and curing of the test specimens. To obtain high strength mortar, condensed silica fume with a powder form and with a gray color was used in all the beams except C1 beam to replace part of the cement used by 10% by weight. The chemical composition of silica fume is given in Table 3. Also for all beams except C1 beam, polypropylene fibers (see Fig. 2) by 900 gm/m^3 of the mortar mix and super plasticizer EDECRETE DM2, complies with ASTM C494-86 with specific weight of 1.05 at 20°C was added to control of ferrocement cracking due to drying shrinkage and thermal expansion/contraction and to lower concrete permeability. Chemical and physical properties of fiber mesh 300-e^3 are shown in Table 4. Also Viscocrete-5930 with 1.0% by weight of cement content was used to increase flowability of the mortar.

Welded wire meshes made from welded galvanized wires with diameter 0.7 mm and with 12.5×12.5 mm size of openings were used as reinforcement in group#4 beams. Also expanded metal wire meshes were used in group#3. These wires are made from steel sheet that has a thickness of 1.25 mm and their diamonds size are 16.5×31 mm. In the group#5, non-metal wire

Table 1 Details of the reinforcements of test specimens

No. Group	No. samples	Reinforcemet wire mesh		Reinforcing steel bars			Total weight of steel (kg)	Volume fraction %
		Type	No. layer	Tens.	Comp.	Stuirr.		
1	C1	-	-	2ϕ10	2ϕ8	6ϕ6/m	4.2737	1.4178
	C2	-	-					
2	FGM1	Fiber glass mesh	1	2ϕ8	2ϕ6	3ϕ6/T.L	3.6607	1.4
	FGM2		2				3.767	1.6219
3	ESM1	Expanded steel mesh	1	2ϕ8	2ϕ6	-	4.4908	1.489
	ESM2		2			-	5.7868	1.9197
	ESM3		1			4ϕ6/T.L	5.21	1.7284
4	WWM1	welded wire mesh	2	2ϕ8	2ϕ6	3ϕ6/T.L	3.0637	1.01635
	WWM2		3				3.4531	1.1455
	WWM3		4			-	3.5017	1.1616
5	PEM1	Poly-ethylene mesh	1	2ϕ8	2ϕ6	3ϕ6/T.L	2.2317	2.07
	PEM2		2				3.5589	3.3751

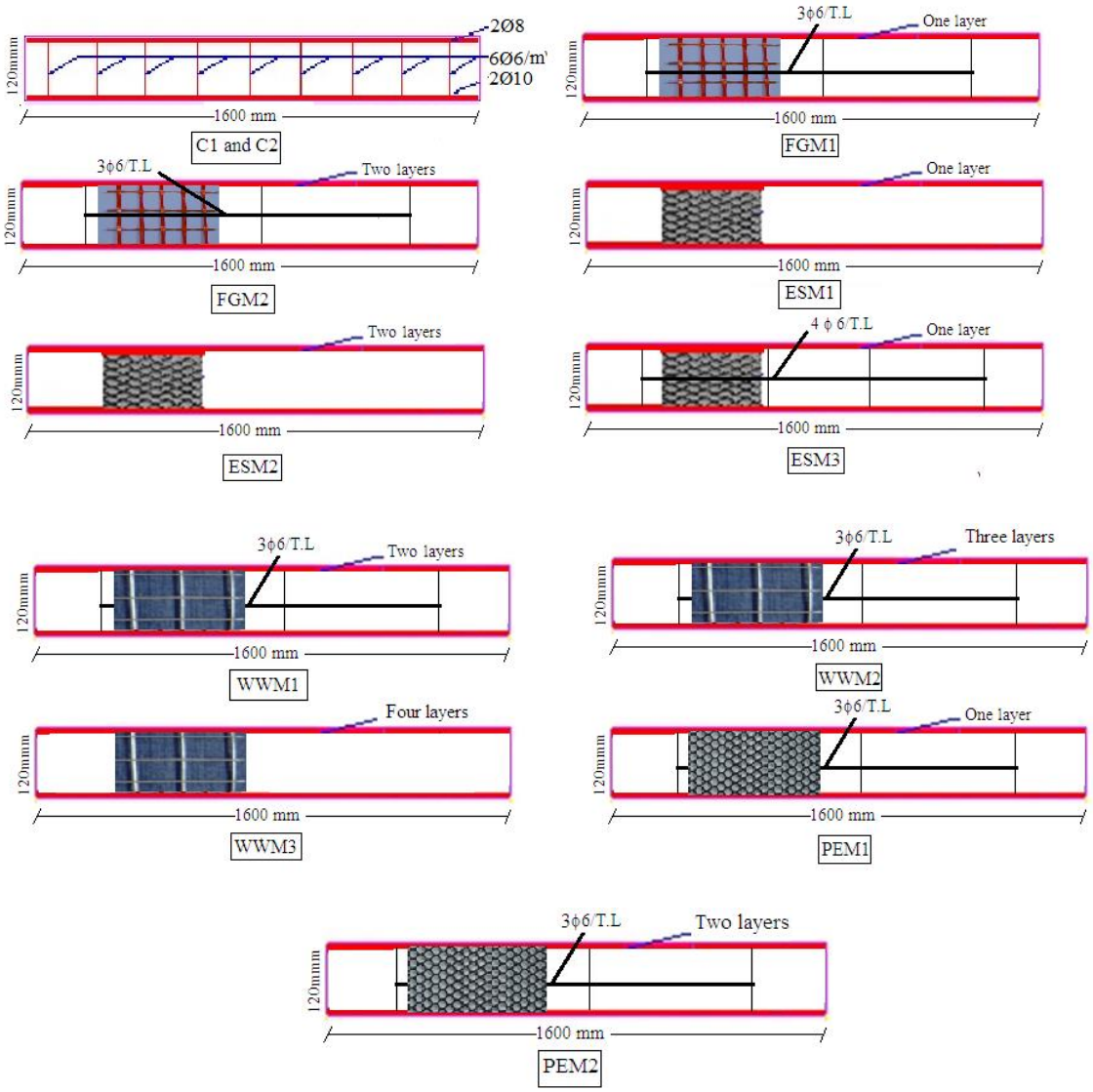

Fig. 1 Details of test specimens

Table 2 Sieve analysis results for the used sand

Sieve Size (mm)	2.83	1.4	0.7	0.35	0.15
% Passing by weight	90.9	79	68	17	2
Limits of (E.E.S.)	100-85	100-75	80-60	30-10	10-0

mesh made from high density polyethylene "Geogrid CE 121" was used. The mesh has 6×8 mm opening size, 3.3 mm thickness, 725 gm/m^2 weight and 2.04% volume fraction. The tensile behavior of polyethylene mesh is considered as 24.7 MPa at extension of 21%. Fiberglass mesh was used in reinforcements of beams in group#2. It was obtained from Gavazzi Company, Italy. It

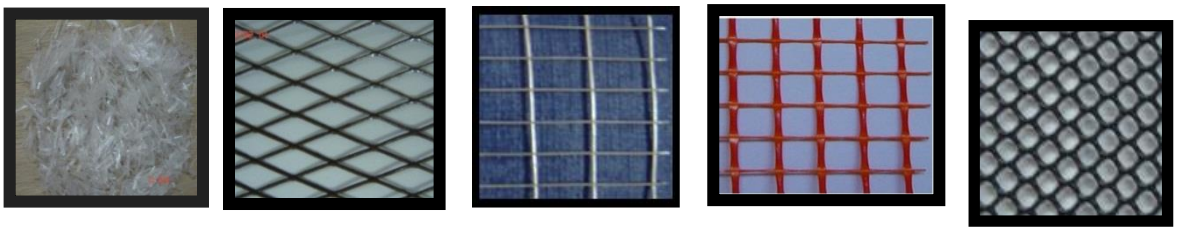

(a) Polypropylene fibers (b) Expanded steel mesh (c) Welded steel mesh (d) Fiber glass mesh (e) Polyethylene mesh

Fig. 2 Used fibers, reinforcement steel meshes and non-metallic mesh

Table 3 Chemical composition of silica fume

Chemical	Weight percent (%)
SiO2	92-94
Carbon	3-5
Fe2O3	0.1-0.5
CaO	0.1-0.15
AL2O3	0.2-0.3
MgO	0.1-0.2
MnO	0.008
K2O	0.1
Na2O	0.1

Table 4 Chemical and physical properties of polypropylene fibers

Absorption	Nil
Specific gravity	0.91
Fiber length	Single cut lengths
Electrical conductivity	Low
Acid & salt resistance	High
Melt point	324℉ (162℃)
Thermal conductivity	Low
Ignition point	1100℉ (593℃)
Alkali resistance	Alkali proof

Table 5 Mechanical properties of wire meshes

Mesh Type	F_y (MPa)	F_u (MPa)	Modulus of Elasticity (GPa)
Expanded mesh	250	350	120
Welded mesh	400	600	170

was available in the Egyptian markets. It is with 12.5×11.5 mm opening dimensions, 1.66×0.66 mm cross section dimensions in the longitudinal direction and 1.0×0.5 mm cross section dimensions in the transverse direction as provided by producing company. The mesh has weight of 123 gm/m^2 and volume fraction of 0.535%. Also it has tensile strength in the longitudinal direction of 32.5 MPa and extension of 5.5% as provided by producing company (refer to Shaheen *et al.*

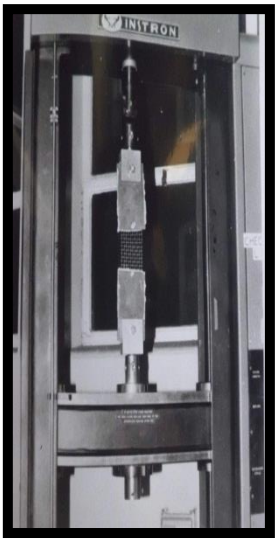

Fig. 3 Wire mesh tensile test

Table 6 Proportions by weight of the ferrocement mortar mix

Material	Weight (kg/m^3)
Cement	650
Sand	1310
Silica fume	(10% replacement of cement content)
Water	230
Superplasticizer	1.0% by weight of (cement+ silica fume)

(2013)). Fig. 2 illustrates all types of the used wire meshes. Three samples of each type of the meshes were tested using the Universal Testing Machine as shown in Fig. 3. The properties of the metal wire meshes are illustrated and shown in Table 5.

2.2 Properties of hardened mortar

The mortar mix was designed according to the ACI recommendations (1980). The mix proportions by weight for mortar per cubic meter are given in Table 6. To estimate the compressive strength of the hardened mortar, twelve 100×100×100 mm cubes were cast and tested after 7 and 28 days according to E.S.S (2011). From the test results, the compressive stress is considered as 22 MPa and 40 MPa after 7 and 28 days; respectively. Three cylinders 50 mm diameter and 100 mm length were used to determine the splitting tensile stress of the selected mortar mix after 28 days. The cylinders axes were laid horizontally in the Hydraulic Compression Testing Machine. From the test results, the indirect splitting tensile strength of used mortar is considered as 4.0 MPa. For control beam C1 (the mortar, the compressive stress is considered as 16 MPa and 30 MPa after 7 and 28 days; respectively.

2.3 Testing of specimen

At the first, the specimens were prepared by preparing the reinforcement. Then the reinforcements were inserted in the wooden forms. After that the morter were mixed by mixing the fine aggregate and cement together in dry state, then 50% of the required water was added followed by the adding of the sillica fume and fiber mesh 300-e^3 and finally the remaining 50% of the required water containing the admixture was added gradually. All the mixing time was about 10 minutes, which was enough to give the homogeneous mixture.Then the mix was cast in the wooden form. The beams were carefully compacted to ensure full compaction. After the molds had been filled with concrete, the surface of concrete in molds was leveled by using the trowel. Finally, the beams were left in the forms for 24 hours in laboratory conditions until the sides of the forms were stripped away.

At the second, the specimens were tested using Flexural Testing Machine of 100 kN capacities. The test was conducted under three-points loadings as shown in Fig. 4. The specimen was centered on the testing machine, where the span between the two supports (two steel rollers) was kept constant at 140 cm. The load is applied at the mid- beam by steel roller (see Fig. 4). The load increment was 5 kN. The deflection at the mid-span of the beams were measured using a dial gauge with an accuracy of 0.01 mm. A set of eight demec points was placed on one side of the specimen to allow measuring the strain versus load during the test. Demec points were placed as shown in Fig. 5.

3. FE Simulation

A general purposed finite element program (ANSYS (2006)) was used in the current research to simulate the tested beams theoretically. Solid65 elements were used for modeling mortar and

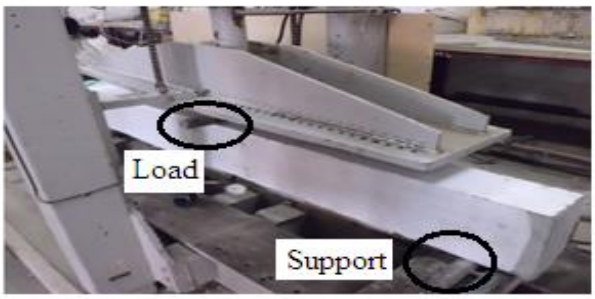

Fig. 4 Specimen test

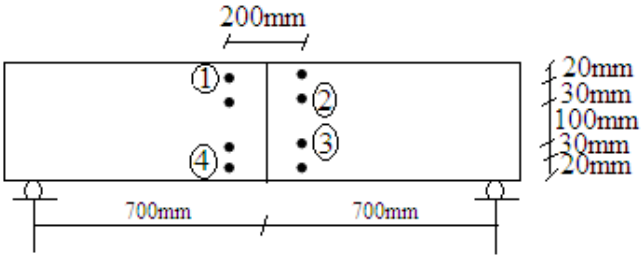

Fig. 5 Locations of demec sets

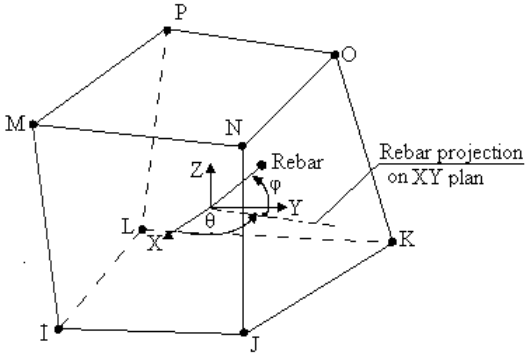

Fig. 6 Solid65 element

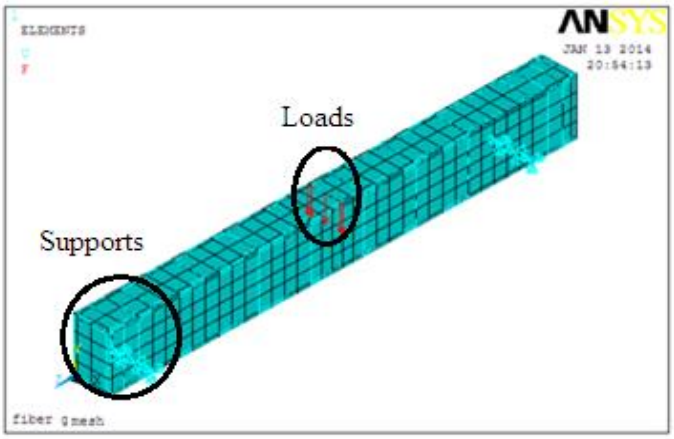

Fig. 7 FE simulation of the tested beam

the wire meshes. Each element is defined by eight nodes. Each node has three degrees of freedom (translations in the nodal *x*, *y*, and *z* directions). This element has one solid material and up to three rebar materials in the three directions. The solid material is used to model the mortar. The rebar capability is used for modeling wire mesh. The wire mesh is specified by its material, volume ratio and orientation angles. The volume ratio is defined as the rebar volume divided by the total element volume. The orientation is defined by two angles in degrees (θ and φ) from the element coordinate system (see Fig. 6). This element has the ability of cracking (in the three orthogonal directions), crushing, plastic deformation, and creep (refer to ANSYS 2006, Hoque 2006, Singh 2006, Shaheen *et al.* 2013). Steel bars and stirrups were modeled by link8 elements. Link8 is a uniaxial tension-compression element with three degrees of freedom at each node: translations in the nodal x, y, and z directions. Plasticity, creep, swelling, stress stiffening, and large deflection capabilities are included. Each support was presented by five hinged supports. The load was concentrated at five joints at the mid-span (see Fig. 7).

The material of the mortar is defined by the compressive, tensile strength of concrete after 28 days, the modulus of elasticity and the multi-linear isotropic stress-strain curve. The modulus of elasticity of concrete and stress-strain curve were employed the Egyptian Code (2007). The modulus of elasticity of concrete (E_c in MPa) can be calculated from Eq. (1) by considering the

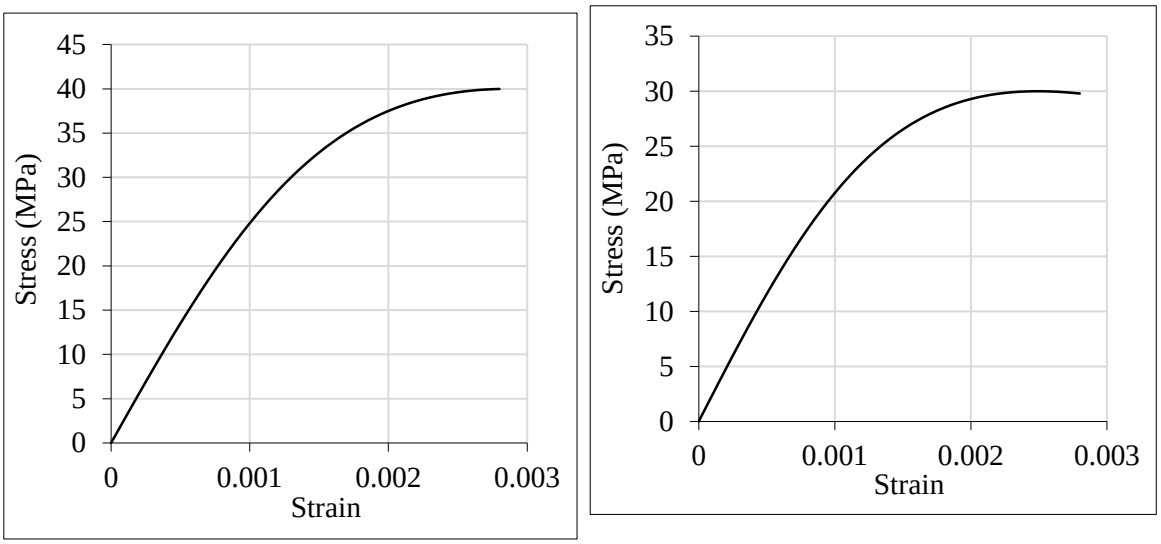

(a) Mortar stress-strain curve of all beams (b) Mortar stress-strain curve of C1 beam

Fig. 8 Stress-strain curve of ferrocement mortar

compressive strength of concrete after 28 days (Fcu in MPa). The multi-linear isotropic stress-strain curve for the concrete can be computed by Eq. (2). The stress-strain curve for the used ferrocement mortar in all tested beam except the first control (C1) beam is presented in Fig. 8 and the modulus of elasticity is considered as 27.8 GPa. The stress-strain curve for the used ferrocement mortar in the first control (C1) beam is presented in Fig. 8 and the modulus of elasticity is considered as 24.1 GPa. The steel and the wire meshes (metal and non-metal) were defined by the yield stress and the modulus of elasticity as illustrated in the experimental work.

$$E_c = 4400\sqrt{F_{cu}} \tag{1}$$

$$Stress = \frac{E_c \varepsilon}{1+(\varepsilon/\varepsilon_0)^2} \tag{2}$$

$$\varepsilon_0 = \frac{2F_{cu}}{E_c} \tag{3}$$

4. Results and discussions

4.1 Experimental results

The behavior of the test specimens in terms of load-deflection relationship, load-strain curve and mode of failure are illustrated and discussed in the current sections. The relationship between the applied load and the central deflection for the tested beams is presented in Fig. 9. From this figure, it can be clearly seen that for all test specimens, the relationship between the load and deflection can be divided into three stages. Elastic behavior until the first cracking, transition stage

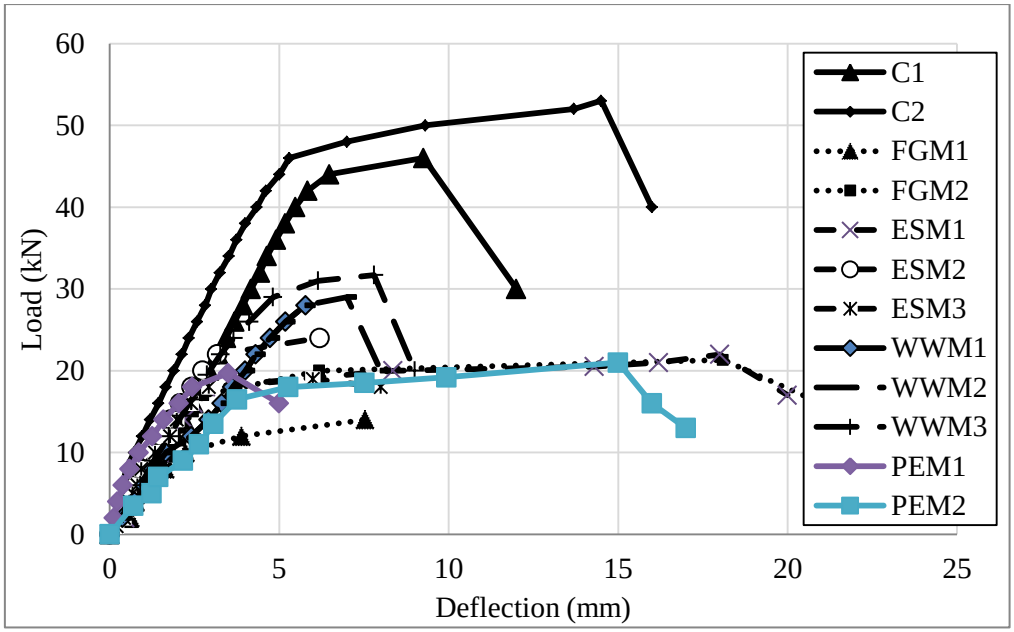

Fig. 9 Load-deflection curves of all test specimens

Table 7 Experimental results

Group No.		Load (kN)			Deflection at ultimate load (mm)	Ductility ratio	Energy absorption (kN.mm)
		Ultimate	First crack	Service			
1	C1	46.1	18	40.67	9.26	2.8492	374.46
	C2	53.2	22	46.35	14.5	6.8075	666.17
2	FGM1	14.6	8	12.94	7.54	4.5697	89.14
	FGM2	21.3	15	19.48	18.1	7.3279	386.2765
3	ESM1	22.1	14	19	18	8.1818	369.63
	ESM2	24.3	18	23.6	6.2	2.562	147.22
	ESM3	19.8	14	18.8	6	3.015	123.005
4	WWM1	24.6	18	24.6	5.27	1.94	121.509
	WWM2	29	18	27.39	7	1.934	144.17
	WWM3	31.7	19.5	30.17	7.8	2.718	198.6375
5	PEM1	19.7	12	19.7	5.8	2.778	74.056
	PEM2	21	14.5	18.06	15	7.075	269.488

and large plastic deformation stage occurred as the result of yielding of the reinforcing bars and the large extension in the reinforcing mesh of the ferrocement beams. Also this figure indicates that early failure occurs in the specimens reinforced with two layers of the fiber glass meshes. Also from these figures, it can be observed that in the beam with polyethylene mesh, the extent of the linear part of the load-deflection curve is very short and the relationship turned to non-linearity before yielding of the reinforcing steel bars. Additionally this figure and Table 7 illustrate that the

beams with one layer expanded wire meshes have the most ductility. Table 7 shows the experimental results of all the tested beams in the tearms of first crack, serviceability and ultimate load, deflection at the failure load, ductility ratio and energy absorption.

The flexural serviceability load was calculated from the load-deflection curves. It is defined as the load corresponding to deflection equal to the span of the beam (1400 mm) divided by constant (constant =250) according to The Egyptian Code (2007). The energy absorption was obtained by calculating the area under the load-deflection curve for each beam. The ductility ratio was calculated as ratio of the mid span deflection at the ultimate load to that at the first cracking load.

From Table 7, it can be noted that control beam C2 has the highest first crack, serviceability and ultimate load and it has the maximum energy absorption. On the other hand the beam reinforced with fiber glass has the lowest first crack, serviceability and ultimate loads. Also this table indicats that the beam reinforced with four layers of welded wire meshes has better structural behavior compared with those beams reinforced with other types of meshes.

The strains of beams were measured at four points; 1, 2, 3 and 4 at mid span of the beam. The relation between the load and strains for all tested beams are presented in Fig. 10 to Fig. 21. For all tested beams, the tensile strain at the gauge location No. 3 and 4 increased with the increase of the applied load. The maximum tensile strain at location No. 3 was more than that at location No. 4. The compressive strain at the gauge location No. 1 and 2 increased with the increase of the applied load. The maximum compressive strain at location No. 2 was less than that at location No. 1. Also from these figures, it can be noticed that C2 beam has the maximum tensial strain and it has the least compressive strain.

The cracking patterns for all the tested beams are shown in Fig. 22. From this figure, it can be clearly seen that the observed cracking patterns for all the tested specimens are flexural cracks and they started in appearing at the beam mid-span. Then they developed rapidly from the tension side towards the compression side and propagated along the beam span with increasing the applied load. Allover, it can be observed that in the two control beams (C1 and C2) shear cracks are generated near the failure load. Also this figure showed that few flexural cracks developed in the specimen GFM1 and their widths at the failure load are seemed to be large than the cracks width in the control beams. Additionally the crack widths are increased with increasing the number of

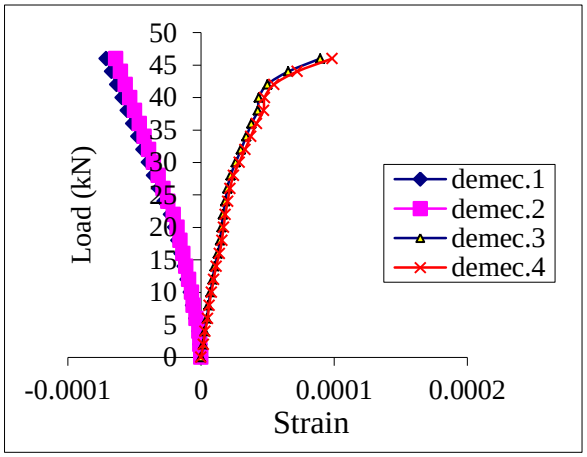

Fig. 10 Load-strain curves of C1

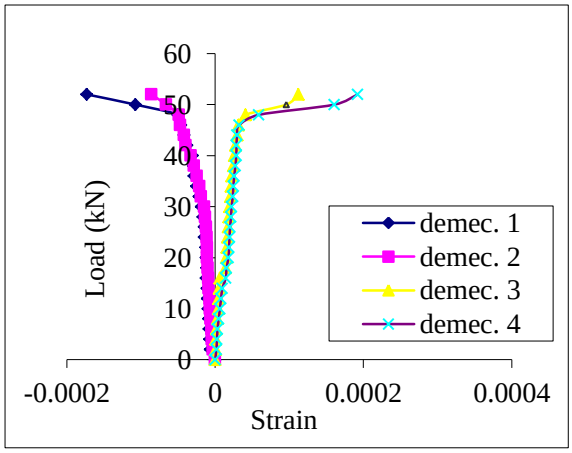

Fig. 11 Load-strain curves of C2

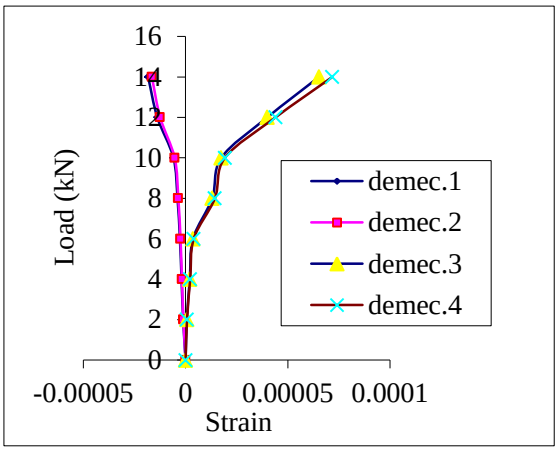

Fig. 12 Load-strain curves of FGM1

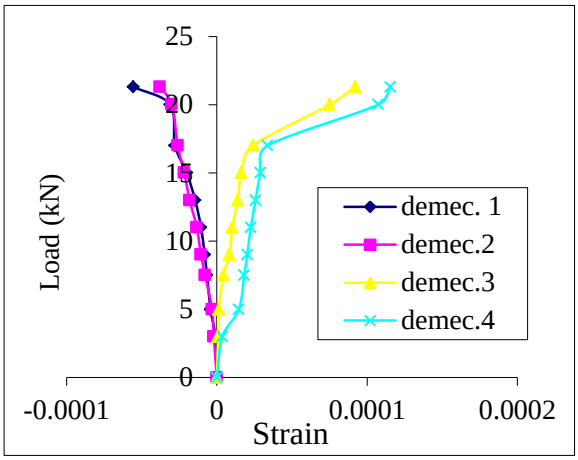

Fig. 13 Load-strain curves of FGM2

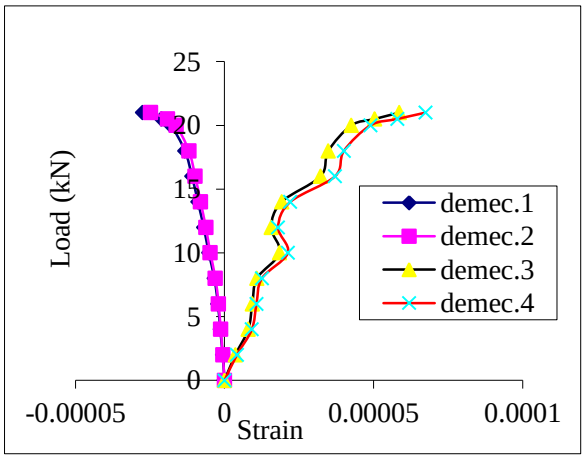

Fig. 14 Load-strain curves of ESM1

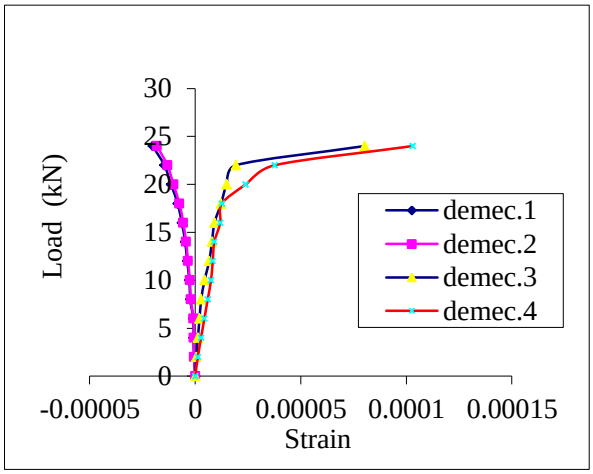

Fig. 15 Load-strain curves of ESM2

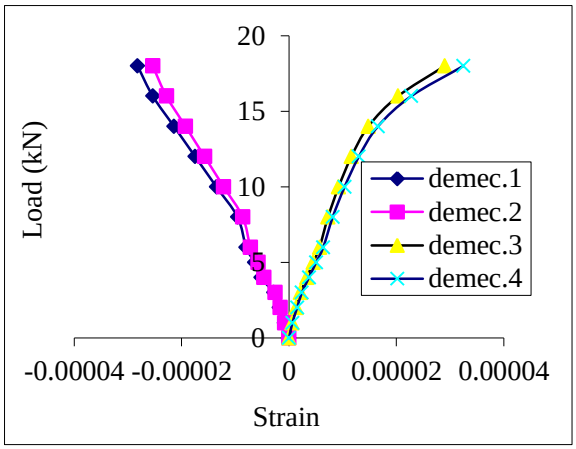

Fig. 16 Load-strain curves of ESM3

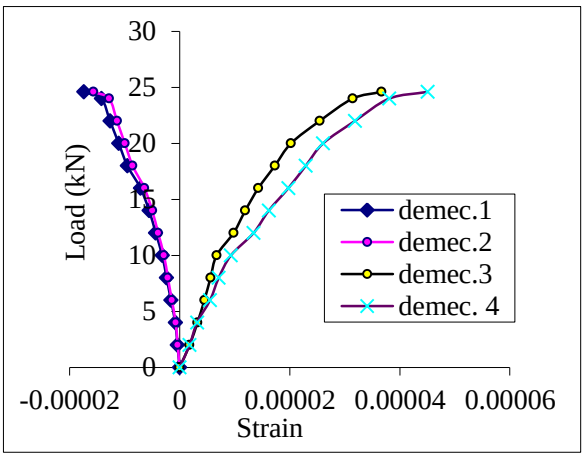

Fig. 17 Load-strain curves of WWM1

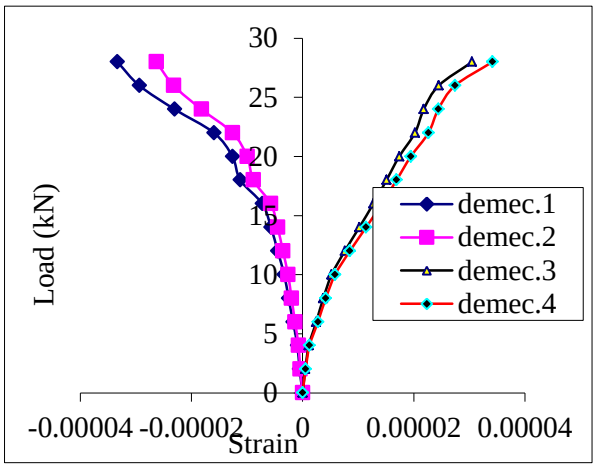

Fig. 18 Load-strain curves of WWM2

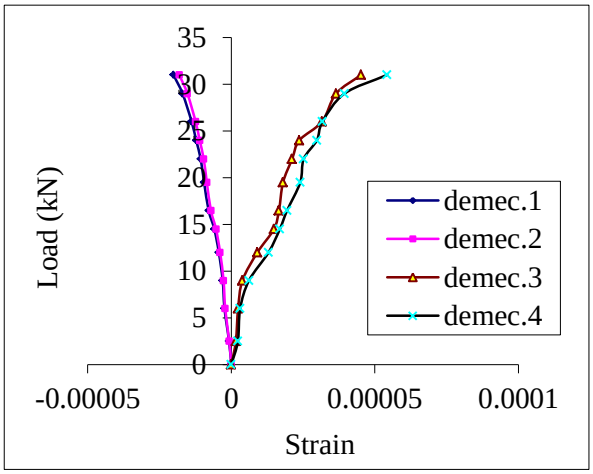

Fig. 19 Load-strain curves of WWM3

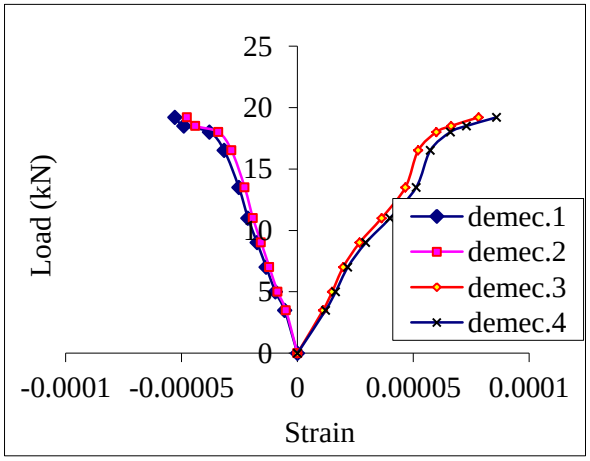

Fig. 20 Load-strain curves of PEM1

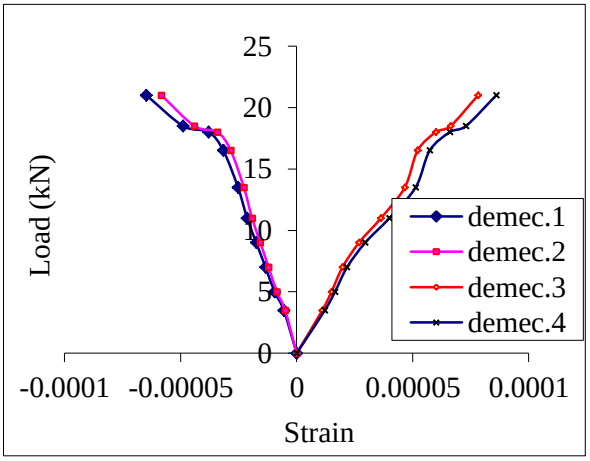

Fig. 21 Load-strain curves of PEM2

layers of fiber fiber glass mesh as indicated in the specimen GFM2. Further more for the beam in group#5, the crack patterns look likes the cracks in group#2. In general the beams which were reinforced with metal wire meshes give smaller crack widths compared with those reinforced with non-metallic meshes.

4.2 Comparison between experimental and FE simulation results

The comparsion between experimental and FE simulation results; ultimate load, mid span deflection at the ultimate load and strain at demec point 1 are illustrated in Table 8. Figs. 23 and 24 present the cracking patterns and applied load-mid span deflection curve; respectively as obtained from the experimental and theoretical results for the second control beam (C2) as the first sample. The comparsion between the experimental and theoretical cracking patterns for FGM2 beam as the

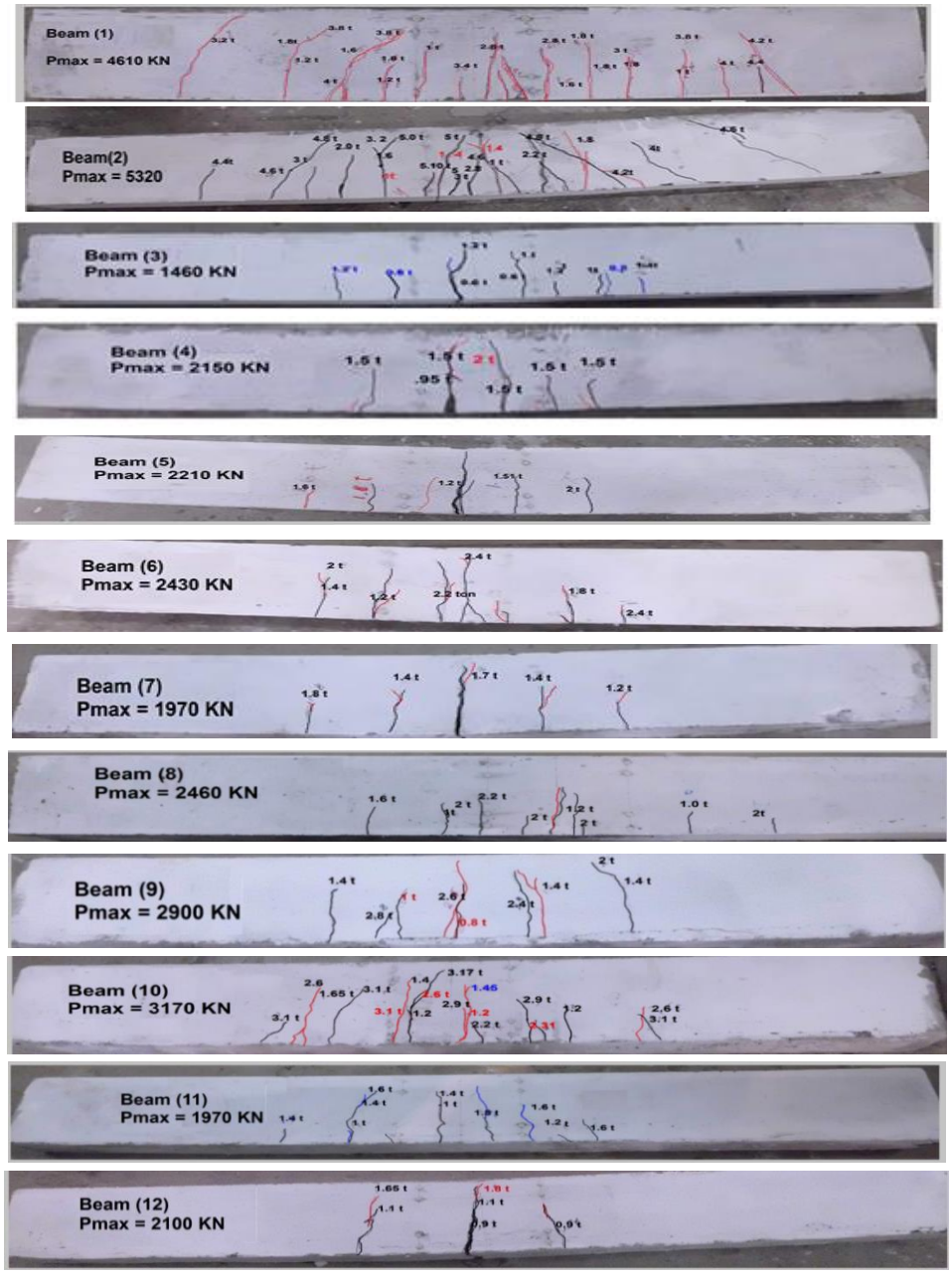

Fig. 22 Cracking patterns of tested beams

second sample are presented in Fig. 25. From Table 8, it can be concluded that the FE simulations for all tested beams give accourete results in comparing with the experimental results. Fig. 26 shows the comparison between experimental and the theoretical applied load-mid span deflection curve for FGM2 beam. Figs. 23 and 25 show the cracking patterns from the FE simulation are similar to the cracking patterns from the experimental work. Figs. 24 and 26 indicate the

Table 8 Comparison between the experimental and FE simulation results

	Ultimate load (kN)		Mid span deflection at ultimate load (mm)		Strain at demec. 1 (Max.)	
	Experimental	FE	Experimental	FE	Experimental	FE
C1	46.1	47.06	9.26	9.91	-0.0000711	-0.0000823
C2	53.2	49.97	14.5	13.83	-0.00017301	-0.002
FGM1	14.6	15.0	7.54	7.72	-1.8328e-05	-1.87e-5
FGM2	21.3	21.88	18.1	17.95	-5.5537e-05	-5.81e-5
ESM1	22.1	20.9	18	18.61	-2.7492e-05	-2.781e-05
ESM2	24.3	26.11	6.2	6.7	-2.0145E-05	-3.062e-05
ESM3	19.8	21.02	6	6.53	-2.8e-05	-3.91e-05
WWM1	24.6	25.32	5.27	5.6	-1.7E-05	-1.812E-05
WWM2	29	30.23	7	7.92	-3.3E-05	-4.102E-05
WWM1	31.7	33.24	7.8	7.31	-2.0145E-05	-1.812E-05
PEM1	19.7	21.37	5.8	5.22	-2.7334E-05	-2.5E-05
PEM2	21	22.16	15	16.1	-0.00005293	-6.801E-05

(a) Experimental

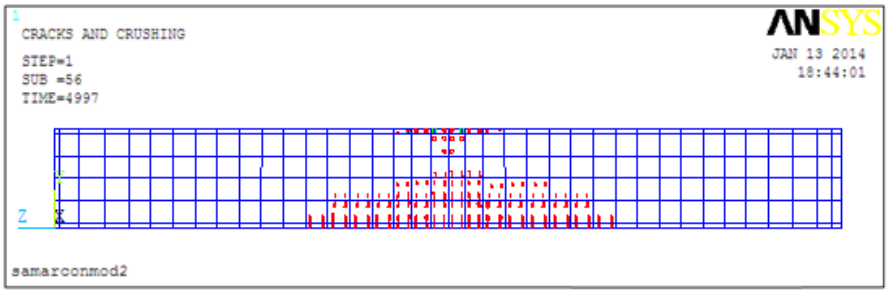

(b) FE simulation

Fig. 23 Cracking patterns of C2 beam from the experimental and theoretical model

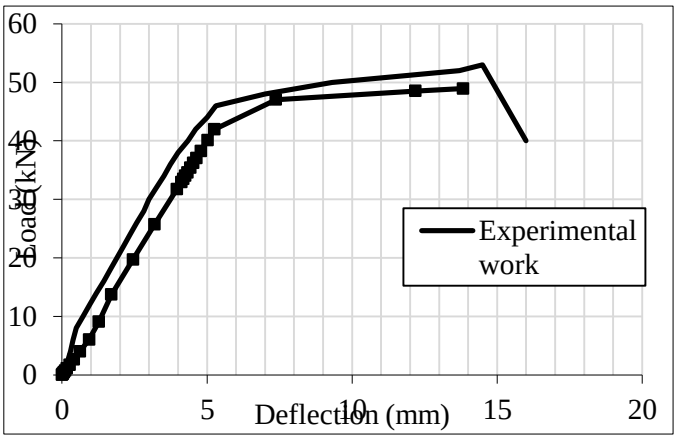

Fig. 24 Experimental and theoretical applied load-central deflection curve for C2 beam

(a) Experimental

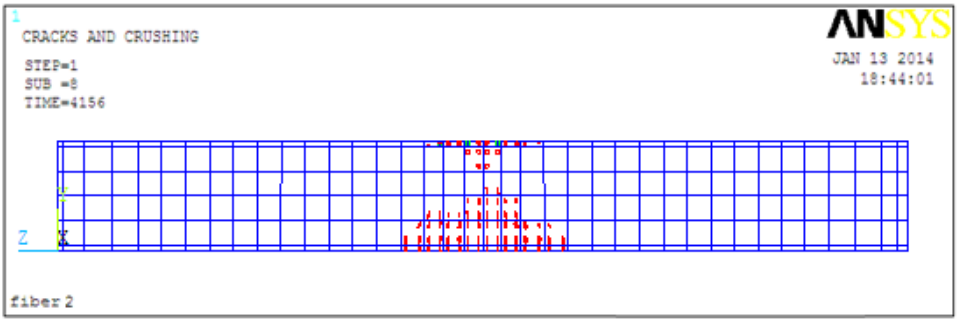

(b) FE simulation

Fig. 25 Cracking patterns of FGM2 beam from the experimental and theoretical model

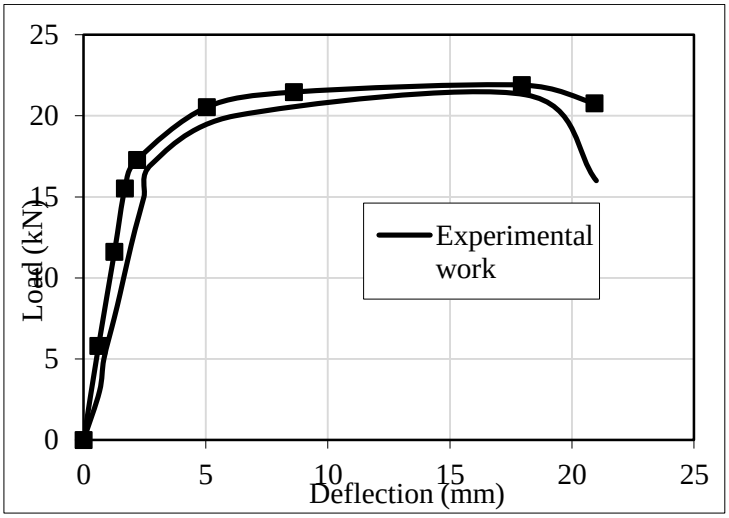

Fig. 26 Experimental and theoretical applied load-central deflection curve for FGM2 beam

relationship between load and deflection are in good agreement in slope of curve in both of linear and nonlinear stages.

5. Conclusions

The main goal of the current research is examining the effect of replacement the traditional reinforcement that is used in ferrocement beams; expanded wire meshes and welded wire meshes with new composite materials. The used composite materials are fiber glass meshes and polypropylene meshes. The effects of using these materials on the structural responses of the proposed beams in terms of failure load, mode of failure, first crack load, serviceability load,

ductility ratio, and energy absorption were studied experimentally. From the experimental results, the following conclusions could be drawn as below:-

• Employing polyproplene fibers in beam C2 achieved the highest first crack load, serviceability load, ultimate load, high ductility and energy absorption properties compared with control beam C1 without polyproplene fibers.

• The ferrocement beam, WWM3 reinforced with four layers of welded wire meshes has better structural behavior compared than the beams reinforced with other types of wire meshes.

• The test beam ESM2 that was reinforced with two layers of expanded wire mesh has the maximum ductility.

• Tested beams reinforced with fiber glass mesh have the lowest first crack loads and ultimate loads.

• Early failure occurs in the specimens reinforced with polyethylene mesh and the extent of the linear part of the load-deflection curve is very short then the relationship turned to non-linearity before yielding of the reinforcing steel bars.

• The cracking patterns occurred in the all beams are flexural cracks. Also the beams reinforced with metal wire meshes emphasized better cracking patterns compared with those reinforced with non metallic mesh this could be attributed to the highest mechanical properties of metallic mesh compared with non metallic mesh.

• Non metallic meshes could be employed for durability applications in corrosive regions.

Also the tested beams were simulated by FE models using ANSYS program. The results of the FE simulation were compared with the experimental results. These comparsion indicated that the FE analysis gives a good outcome compared to the experimental tests.

References

Aboul-Anen, B., El-Shafey, A. and El-Shami, M. (2009), "Experimental and analytical model of ferrocement slabs", *Int. J. Rec. Trend. Eng*., IJJCE, Oulu, Finland, **1**(6), 25-29.

Ali, A. (1995), "Applications of ferrocement as a low cost construction material in malaysia", *J. Ferrocemen*, **25**(2), 123-128.

Al-Kubaisy, M.A. and Jumaat, M.Z. (2000), "Flexural behavior of reinforced concrete slabs with ferrocement tensionz cover", *J. Constr. Build. Mater.*, **14**, 245-252.

Robles-Austriaco, L., Pama, R.P. and Valls, J. (1981), "Ferrocement an innovative technology for housing", *J. Ferrocement*, **11**(1), 23-47.

Elavenil, S. and Chandrasekar, V (2007), "Analysis of reinforced concrete beams strengthened with ferrocement", *Int. J. Appl. Eng. Res.*, **2**(3), 431-440.

Fahmy, E.H., Shaheen, Y.B. and Korany, Y.S. (1997), "Use of ferrocement laminates for repairing reinforced concrete slabs", *J. Ferrocement*, **27**(3), 219-232.

Jumaat, M. and Alam, A. (2006), "Flexural strengthening of reinforced concrete beams using ferrocement laminate with skeletal bars", *J. Appl. Sci. Res*., **2**(9), 559-566.

Kaish, M.A., Alam, A.B., Jamil, M.R., Zain, M.F. and Wahed, M.A. (2012), "Improved ferrocement jacketing for restrengthening of square RC short column", *J. Constr. Build. Mater*., **36**, 228-237.

Mourad, S.M. and Shannag, M.J. (2012), "Repair and strengthening of reinforced concrete square columns using ferrocement jackets", *J. Cem. Concrete Compos*., **34**, 288-294.

Xiong, G.J., Wu, X.Y., Li, F.F. and Yan, Z. (2011), "Load carrying capacity and ductility of circular concrete columns confined by ferrocement including steel bars", *J. Constr. Build. Mater*., **25**, 2263-2268.

Naaman, A.E. and Shah, S.P. (1971), "Tensile test of ferrocement", *ACI J. Proceed.*, **68**(9), 693-698.

Rajagoplan, K. and Parameswaran, V.S. (1975), "Analysis of ferrocement beams", *J. Struct. Eng.*, **2**(4), 155-

164.
Walker, P. (1995), "Moment-curvature relations for ferrocement beams", *J. Ferrocement*, **25**(4), 347-359.
Nassif, H. and Najm, H. (2004), "Experimental and analytical investigation of ferrocement-concrete composite beams", *J. Cem. Concrete Compos*., **26**, 787-796.
Daniel, I. and Shah, P. (1994), "Fiber reinforced concrete, developments and innovations", *Am. Concrete Ins.*, **142**, 318-326.
Al-sayed, H. and Al-hozaimy, M. (1999), "Ductility of concrete beams reinforced with FRP bars and steel fibers", *J. Compos. Mater*., **33**(19), 1792-806.
Harris, G., Somboonsong, W. and Ko, K. (1998), "New ductile hybrid FRP reinforcing bar for concrete structures", *J. Compos. Constr*., **2**(1), 28-37.
Li, C. and Wang, S. (2002), "Flexural behaviors of glass fiber-reinforced polymer (GFRP) reinforced engineered cementitious composite beams", *J. Mater*., **99**(1), 11-21.
Qu, W., Zhang, X. and Huang, H. (2009), "Flexural behavior of concrete beams reinforced with hybrid (GFRP and steel) bars", *J. Compos. Constr*., **13**(5), 350–359.
Sakthivel, P. and Jagannathan, A. (2012), "Study of flexural ferrocement and thin reinforced cement behavior of ferrocement slabs reinforced with PVC-coated weld mesh", *Int. J. Eng. Res. Develop.*, **1**(12), 50-57.
Sakthivel, P. and Jagannathan, A. (2012), "Fibrous ferrocement composite with PVC-coated weld mesh and bar-chip polyolefin fibers", *Int. J. EOMATE*, **3**(2), 381-388.
Shaheen, Y., Soliman, N. and Hafiz, A. (2013), "Structural behavior of ferrocement channels beams", *J. Concrete Res. Lett.*, **4**(3), 621-638.
E.S.S (2011), *Egyptian Standard Specifications for Plain and Reinforcement Concrete*, Egypt, No. 2070-2007.
ACI Committee 549 (1980), State-of-the-art report on ferrocement, American Concrete Institute, Vol. 4, No. 8.
ANSYS (2006), "Help and manual", 12th Editor, ANSYS Inc, PA, USA.
Hoque, M. (2006), "3D nonlinear mixed finite-element analysis of RC beams and plates with and without FRP reinforcement", M.Sc. Thesis, University of Manitoba, Winnipeg, Manitoba, Canada.
Singh, G. (2006), "Finite element analysis of reinforced concrete shear walls", M.Sc. Thesis, Deemed University, India.
Shaheen, Y.B.I., Eltaly, B. and Kameel, M. (2013), "Experimental and analytical investigation of ferrocement water pipe", *J. Civil Eng. Constr. Tech*., **4**(4), 157-167.
E.C.P. (2007), Egyptian code of practice: design and construction for reinforced concrete structures, Research Centre for Houses Building and Physical Planning, Cairo, Egypt, No. 203.